THE HIGH TEMPERATURE OXIDATION OF TANTALUM AND TANTALUM CARBIDE IN HYPERSONIC-RELEVANT CONDITIONS

Connor J. Stephens, Elizabeth J. Opila
University of Virginia
Department of Materials Science and Engineering

Abstract

The oxidation of Ta and TaC was studied via Joule heating in a custom resistive heating system at 1300, 1400, and 1500°C for up to 10 minutes in a 1%O_2-Ar environment. Oxidation was found to proceed linearly with time for both materials. Gas-phase diffusion through large defects is identified as the limiting transport process below 1500°C because the oxide on Ta is highly cracked. At 1500°C, the oxide becomes denser and oxidation slows. The Ta oxidation rate decreases with increasing temperature because the oxide becomes more protective. The oxide on TaC is highly porous due to CO(g) formation during oxidation. While the porosity decreases as temperature increases, these defects prevent the oxide from becoming protective as temperature increases. Additionally, a new resistive heating system equipped with a microplasma capable of dissociating oxygen was constructed. The capabilities of this system are shown by Ta oxidation experiments in molecular and atomic oxygen. Oxidation increases in atomic oxygen when the oxide on Ta is non-protective.

Introduction

During hypersonic flight (>Mach 5), leading-edge (LE) components, such as nose caps and wing LEs, are exposed to temperatures above 2000°C[1]. Additionally, high temperatures coupled with the shockwaves created during high Mach flight can dissociate molecular oxygen (MO) into atomic oxygen (AO). LE components must be made of materials which can withstand such harshly oxidizing environments. State-of-the-art high temperature materials systems are Si-based because of the highly protective nature of SiO_2 against oxidation. However, SiO_2-based materials are limited by the melting point of SiO_2 (T_M=1723°C) and begin to actively oxidize to form SiO(g) at T>1600°C[2]. There is a significant push to replace Si-based materials with new, long-life, "ultra-high" temperature (T>1723°C) materials.

a. Oxidation of Transition Metals and Carbides

The transition metals, M, and metal carbides, MC (M = Ti, Zr, Hf, Ta) form oxides which have melting points greater than the melting point of SiO_2 (1723°C). The carbides are considered candidate materials for leading-edge hypersonic components because they have high melting temperatures (>3000°C). However, they are often expensive and challenging to manufacture. The metals, on the other hand, are much more cost-effective and simpler to manufacture, but have significantly lower melting temperatures.

Both the metals and carbides have poor oxidation resistance at high temperatures and the mechanisms which drive oxidation are not well understood. Conventional understanding of these materials would indicate that the carbides should oxidize more rapidly because the CO(g) which forms during oxidation creates a porous oxide and allows for rapid oxygen ingress to the substrate, whereas the metals will tend to form dense oxides which protect against oxygen ingress.

However, there are many mechanisms by which the rate or pathway of oxygen ingress may be changed at high temperatures, such as non-stoichiometry in the oxide[3,4] or carbide[5,6], oxide sintering[7–9], phase transformations of the substrate[10] or oxide[11–13], oxycarbide formation[7,14–17], change in oxide plasticity[18–20], and grain boundary oxidation[21,22]. This list is incomplete but gives a picture of the complexity presented during the high temperature oxidation of metals and metal carbides. Despite the wide body of literature regarding these materials, the effect of carbon on the oxidation mechanism of the metals as compared to the carbides is not well documented. No direct comparisons of the metals and carbides in identical experimental

conditions have been conducted to isolate the role of carbon on the oxidation process.

b. Oxidation in Atomic Oxygen

Oxygen dissociation occurs before oxygen adsorption in the oxidation process. However, if the oxygen is already dissociated, the energy barrier to oxidation would be lower and the oxidation rate may increase. Despite this potential impact, very few studies have been conducted for the high temperature oxidation of materials in AO. This is primarily because of the prohibitively expensive operating costs of the facilities traditionally used to generate AO in high temperatures, such as arc-jets and plasmatrons (>$150K/day to operate, >$1M to build). Alternate methods, such as microwave-generating AO furnaces, suffer from low AO fluence due to recombination at chamber walls[23]. These technologies also do not allow for the separation of AO effects from high temperature, pressure, or flow velocity. A new technique is needed to isolate the effects of AO on oxidation at high temperatures.

Some work has been conducted on relevant high temperature materials systems. Balat et al. studied the oxidation of SiC in MO and microwave-generated AO[24]. They observed the passive to active transition (SiO_2 to SiO(g)) occurs at a lower Po_2 for AO as compared to MO. Thus, SiC can retain a passivating scale at higher temperatures in AO than in MO and could survive in highly oxidizing environments longer if the environment contains AO. This effect is contradictory to thermodynamic predictions and suggests kinetic control of the active-to-passive transition in SiC.

The oxidation of ZrB_2 and ZrB_2-SiC, which form glassy boria or borosilicate scales have also been investigated in AO containing environments. Monteverde and Savino explored ZrB_2-SiC up to 2000°C in an arc-jet and found ZrB_2-SiC to have low recombination catalycity and good survivability during re-entry condition testing but reported no specific effects of AO on oxidation[25]. Marschall et al. compared ZrB_2-SiC oxidation in a plasmatron to oxidation in a traditional box furnace from 1250-1575°C[26]. They reported faster SiO_2 growth and slower volatilization, and also found an increased passive regime of the borosilicate glass in AO, in good agreement with Balat's results for SiC. Li et al. qualitatively showed that the oxidation rate at

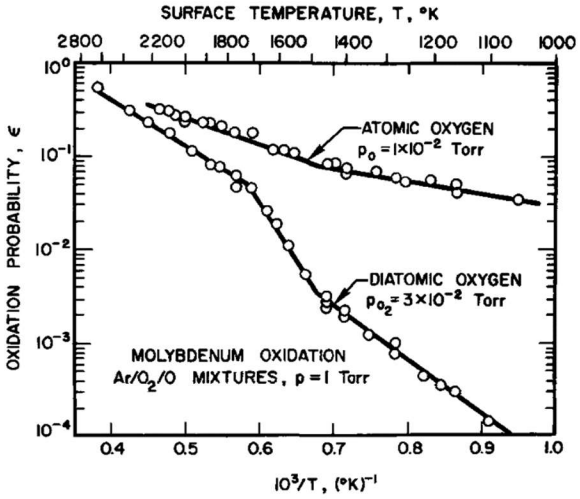

Figure 1: Comparison of the oxidation probabilities of Mo in molecular oxygen and atomic oxygen. Reproduced from Rosner and Allendorf[28].

1500°C is largely pressure dependent and increases when AO is present[27].

Very little AO oxidation studies have been conducted on transition metals or carbides. Rosner and Allendorf have shown that the oxidation of Mo and W[28] and carbon[29] are more rapid in AO (Figure 1). However, these materials form gaseous oxides and leave the underlying material exposed to the AO at all times. The oxidation of materials which form condensed phases in AO has not been widely studied.

The goal of this work is to 1) explore the oxidation of early transition metals and their carbides in identical experimental conditions to elucidate the role of carbon on the oxidation process; 2) construct a new, cost-effective experimental system for high temperature oxidation which will enable the comparison of molecular oxygen and atomic oxygen environments; and 3) investigate the differences in oxidation mechanisms and kinetics of the transition metals and carbides in molecular oxygen and atomic oxygen environments. For brevity, this report will focus only on the oxidation of Ta and TaC.

Experimental Methods

a. Custom Resistive Heating System

Oxidation in MO was conducted using a custom **resistive heating system (RHS)**, based on the design of Karlsdottir and Halloran[30] and modified by Shugart and Opila[31]. A schematic

(a)

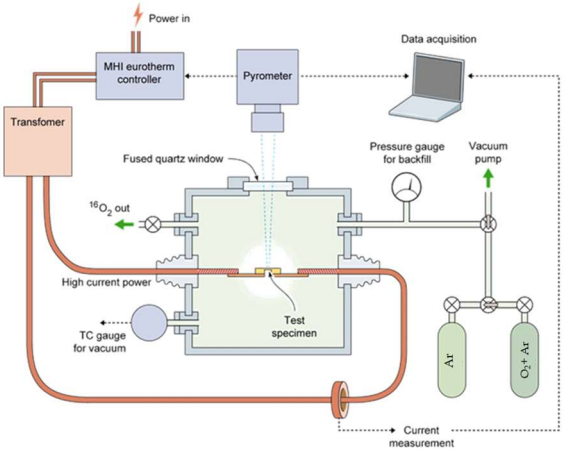

(b)

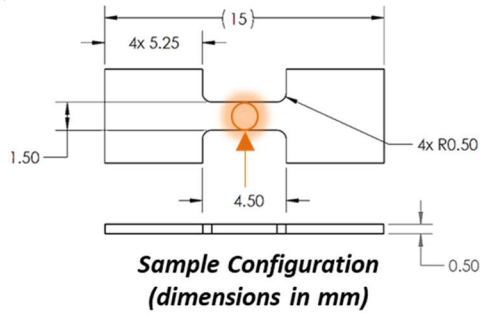

Figure 2: Schematic diagrams of (a) the custom RHS at UVA and (b) the sample geometry used in the RHS.

of the RHS is shown in Figure 2a. Approximately 100A of current is passed through the "dogbone" shaped samples. The reduced cross section causes Joule heating which is localized to a "hot zone" (Figure 2b, orange circle) in the center of the samples. Because this area of the sample is not in contact with anything, reactivity with experimental components is minimized. Current is delivered by a power supply unit equipped with a Eurotherm controller (BPAN-O-PLUS, Micropyretics Heaters International, Inc., Cincinnati, OH) in a control loop with an emissivity-correcting pyrometer (Pyrofiber Lab, Pyrometer Instrument Co., Windsor, NJ). The power output is adjusted until the desired temperature is reached. Temperature control can be maintained below 1800°C with an accuracy of ±20°C at 1300°C and ±50°C at 1800°C. Pt foil and Y-stabilized ZrO_2 (YSZ) padded alligator clips are used to maintain good sample connection and to prevent reaction between the electrical leads and the sample during heating.

b. Microplasma Resistive Heating System

High-pressure DC hollow-cathode discharges, more commonly referred to as microplasmas (MPs), are a type of plasma where at least one dimension is smaller than 1mm[32]. It is shown here that the characteristics of these plasmas allow for the cost-effective production of AO for ultra-high temperature oxidation testing. The characteristics of MPs are as follows:

1. Near-atmospheric pressure stability (1-100 Torr magnitudes); allows for use of standard laboratory vacuum equipment to achieve discharge, reducing cost.
2. A non-Maxwellian, high-tail electron energy distribution function (EEDF); more high-energy electrons in the plasma provide greater probability of dissociative collisions, increasing the flux of AO.
3. Non-equilibrium thermodynamics ($T_{ion} << T_{electron}$); the high surface-area-to volume ratio of MPs quenches the ions, resulting in a "cold plasma" (~100°C) and allowing separation of the effects of temperature from plasma.

By flowing a gas through a capillary with sufficient potential across it, an MP jet is formed. Designing a new RHS to incorporate an oxygen MP jet allows for ultrahigh temperature AO oxidation studies.

The RHS in the Opila lab at the University of Virginia utilizes five out of the six available flanges of its cube-shaped chamber. A new RHS was designed which utilizes the sixth and final flange on the bottom of the chamber to incorporate a MP. The system has the same functionality but can achieve higher temperatures (up to 2500°C) and create AO. AO production was confirmed by plasma emission spectroscopy. The dissociation efficiency of the MP is estimated at 33±9% by Kapton HN erosion[33] following ASTM E2089-15(R20). To differentiate this new RHS from the old, it will be referred to as the **microplasma resistive heating system (MRHS)**. The MP used in the MRHS was designed after the one reported by Koh, O'Hara, and Gordon for thin film synthesis[34,35]. A schematic of the functioning MRHS and a

(a)

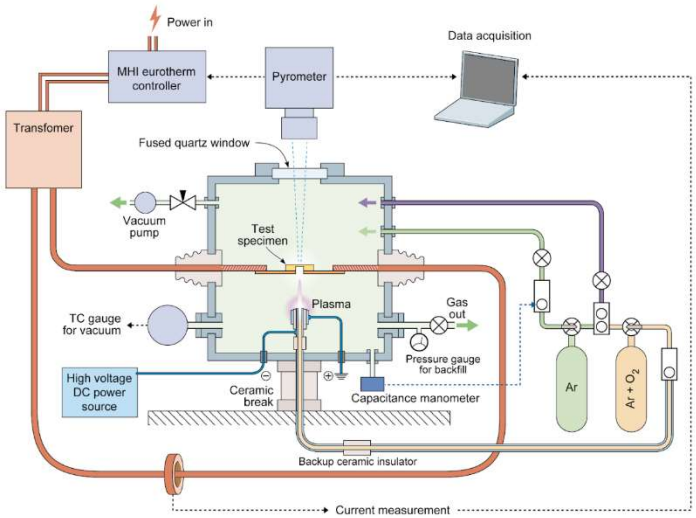

(b)

Figure 3: (a) Schematic diagram of the new MRHS at UVA and (b) the operating MP in the MRHS.

picture of the MP in operation are shown in Figure 3a and 3b, respectively.

c. Materials

A sheet of 0.635mm (0.025 in.) thick Ta (99.5% pure, metals basis) was sectioned via electrical discharge machining (Exothermics, Inc., Amherst, NH, USA) into the "dogbone" sample geometry shown in Figure 2b. Three-inch TaC pucks produced by hot isostatic pressing (Kurt J. Lesker Company, Pittsburg, PA) were diamond machined (Bomas Machining Specialties, Inc., Woburn, MA) into the dogbone geometry of 0.5mm (0.020 in) thick. Archimedes method indicated the TaC to be ~99.3% of theoretical density.

Additionally, instrumental gas analysis (IGA) was used to verify the carbon content of the unoxidized carbide (Evans Analytical Group, Syracuse, NY), and high-resolution transmission electron microscopy (TEM; Themis-Z STEM, Thermo Fisher Scientific, Waltham, MA) and selected area electron diffraction (SAED) were used to probe the crystallinity of the carbide. TaC has a large range of carbon stoichiometries which are possible, ranging from Ta_2C to TaC. IGA indicated ~6.2wt% C, which correlates to ~49.9at% C (TaC_x, x=99.8). TEM/SAED verified that the resulting carbon signal is all from the carbide phase and not from any free, amorphous carbon. Thus, all oxidation results for TaC correspond with the monocarbide phase.

d. Experimental Method

Literature on Ta and TaC oxidation at near atmospheric Po_2 is reported up to 1300°C[13,36]. Thus, oxidation experiments were conducted at 1300°C, 1400°C, and 1500°C for up to 10 min. In some cases, especially in the carbides, samples would break before the set end time. Because this stops current flow, these samples were still included in the data set with an end time at the time of fracture. Samples were ramped to temperature at 5°C/sec in pure Ar. Atmospheric pressure gas flowed at 950-1000 sccm for the duration of each experiment. Once at the desired temperature, the gas was switched to a flowing 1% O_2-Ar mixture. Oxidation time started when oxygen was introduced to the system, and current flow was stopped at the end time of the experiment. When the current is stopped, the sample cools to near room temperature in only a few seconds.

Oxidation experiments in the MRHS were similar, with the exception of MP operation. MPs require a reduced pressure to operate, so the MRHS maintains a fixed background pressure of 65 torr of pure Ar during oxidation. In AO-containing experiments, 15mA and 300-500V were applied across the MP while 100 sccm of 1% O_2-Ar flowed from the capillary. Because of the dissociation efficiency, the gas composition in AO+MO exposures is assumed to be 0.33%O-0.66%O_2-Ar at 65 torr.

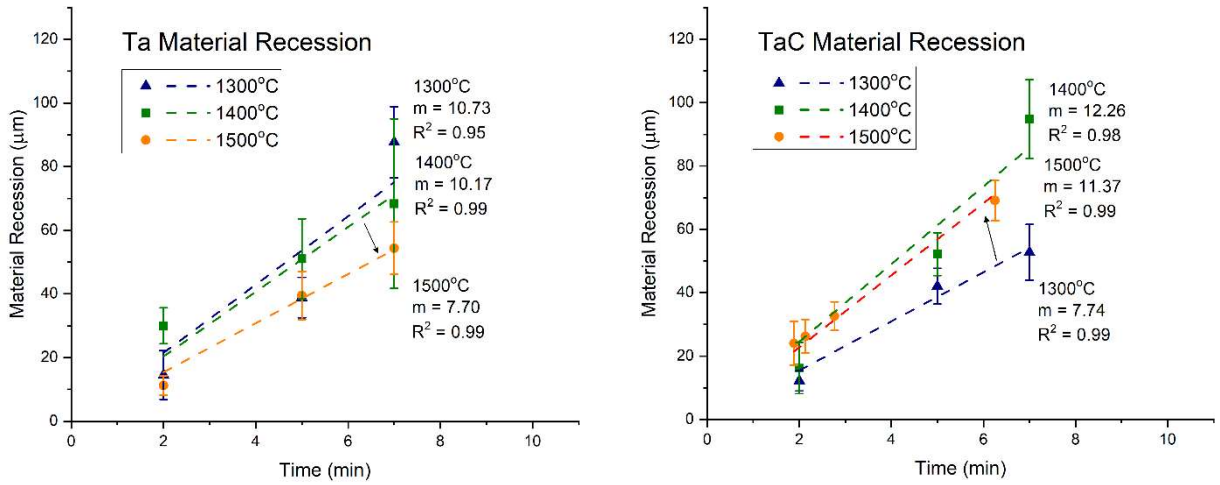

Figure 4: Oxidation kinetics for Ta and TaC at 1300-1500°C in 1%O_2-Ar. The black arrows follow the direction of increasing temperature to highlight the abnormal behavior for Ta oxidation at 1300°C.

Experimental conditions were kept identical, including the background pressure, whether the MP was on or off.

Samples were characterized using scanning electron microscopy (SEM) and X-ray diffraction (XRD). Oxidation kinetics were determined from cross section measurements of the base material recession and oxide thickness. Recession is used to compare different materials, as factors like oxide sintering and differences in molar volume upon oxide growth can skew oxide thickness measurements. Data points represent the average of at least two samples with 10-20 points from the middle third of each sample (measured via ImageJ[37]).

To better understand the oxygen transport mechanism through the scales, Ta samples were also oxidized in the RHS at 1300°C and 1400°C for 4.5 min, followed by a second oxidation in $^{18}O_2$ (97% enriched, Sigma Aldrich, Saint Louis, MO) for 6 sec and 20 sec, respectively. Time was not kept strictly because the purpose of these experiments was to identify oxidation pathways, not measure kinetics. These "double oxidation" samples were cross sectioned and analyzed via time-of-flight secondary ion mass spectrometry (TOF-SIMS; TOF-SIMS V, ION TOF, Inc., Chestnut Ridge, NY; C. Zhou, North Carolina State University).

Results

a. Ta and TaC Oxidation in the RHS

The recession of the base material is plotted versus time for Ta and TaC in Figure 4. Due to

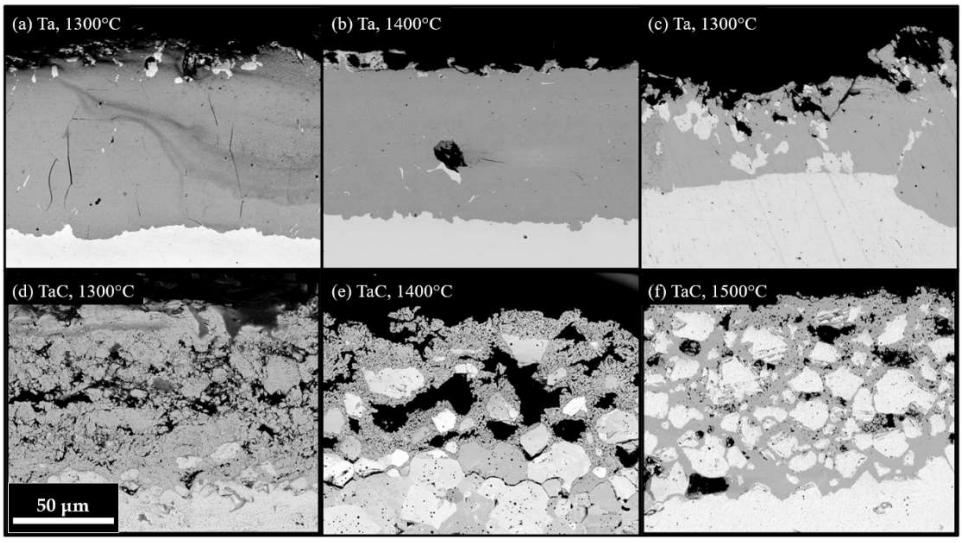

Figure 5: Polished oxide cross sections for Ta and TaC after oxidation for 5 minutes in 1%O_2-Ar.

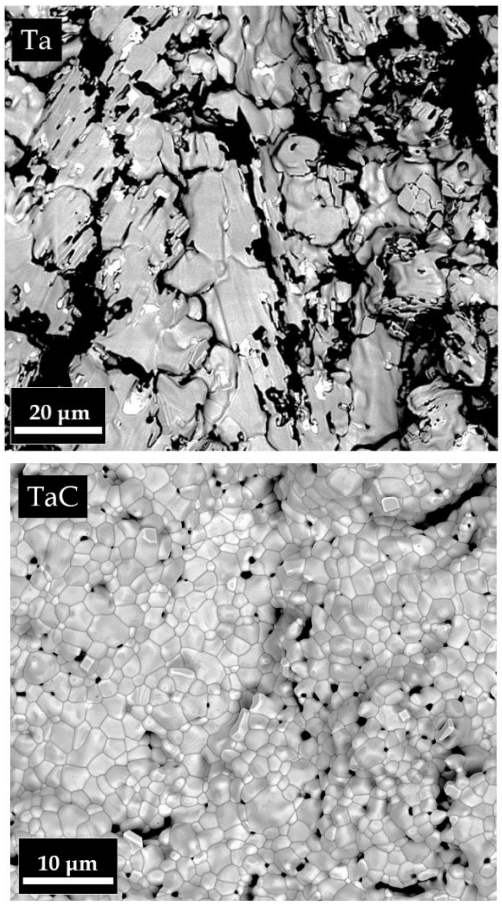

Figure 6: Backscatter SEM plan view micrographs of the oxides formed on Ta and TaC after 5 min oxidation at 1400°C in 1% O_2 – Ar.

the large error bars on the data, several oxidation rate laws could be fit to the recession data. Kinetics are plotted with linear time for simplicity. A series of polished cross section micrographs for Ta and TaC after oxidation after 5min at 1300-1500°C in 1% O_2-Ar are shown in Figure 5. Ta exhibits a cracked, adherent oxide with decreasing amounts of cracks as temperature increases. Ta metal can be found trapped inside the oxide at all temperatures. TaC exhibits a highly porous oxide with large voids throughout. Additionally, carbide grains can be seen being lifted out via a grain boundary oxidation mechanism. The degree of grain boundary oxidation and grain lift-out increases as temperature increases. Additionally, the degree of porosity in the oxide decreases with increasing temperature. Plan view micrographs of the oxides grown on Ta and TaC after oxidation at 1400°C for 5min are shown in Figure 6. The oxide on Ta forms as large plates with Ta metal interspersed. The oxide formed on TaC forms as small, rounded grains with intergranular pores. XRD data (not shown) indicates that the oxides formed on Ta and TaC are the same oxide phase.

$^{18}O_2$ isotope maps from TOF-SIMS on the Ta "double oxidation" experiments are shown in Figure 7. The surface of the oxide is saturated with $^{18}O_2$. Additionally, there is a significant signal of $^{18}O_2$ near the metal/oxide interface,

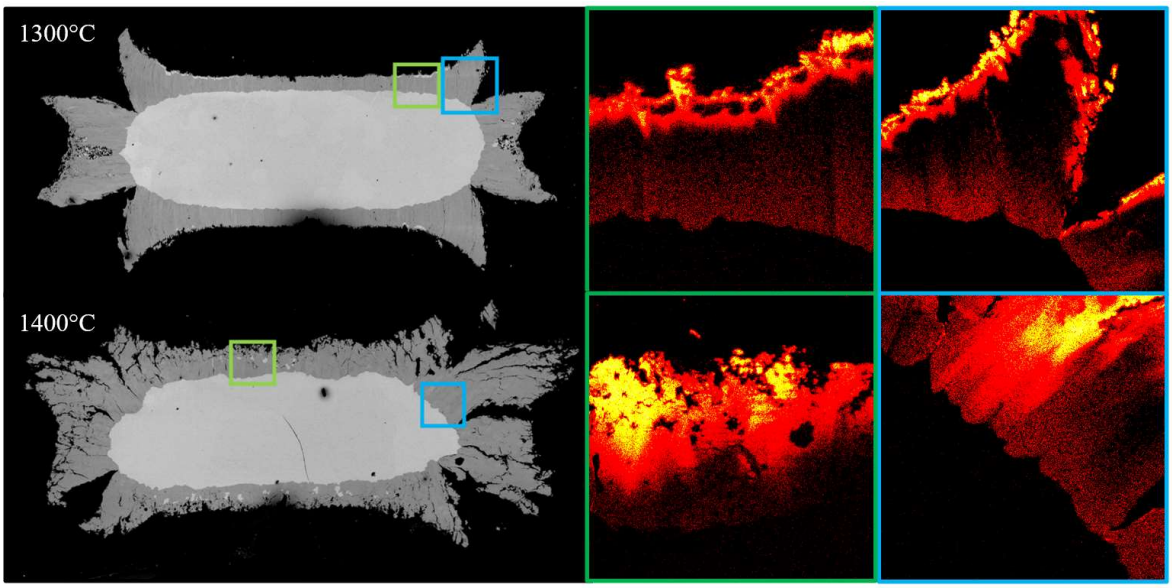

Figure 7: Polished cross sections and TOF-SIMS 18O isotope maps of after tracer oxidation for 4.5 minutes in 16O2. Top row oxidized for 6 seconds in 18O2 at 1300°C, bottom row oxidized for 20 seconds in 18O2 at 1400°C. Results courtesy of C. Zhou (North Carolina State University).

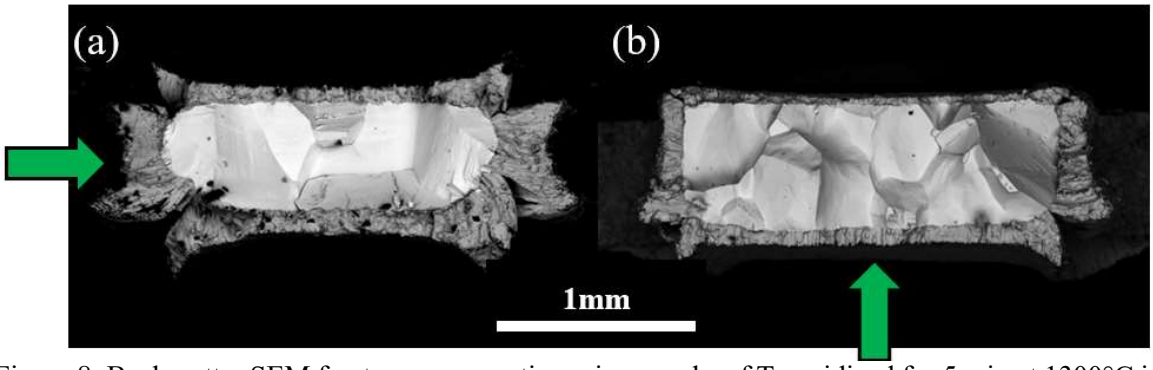

Figure 8: Backscatter SEM fracture cross section micrographs of Ta oxidized for 5 min at 1300°C in 1% O_2 – Ar using (a) the original RHS with a 1000 sccm flow rate and (b) the new MRHS with a 100 sccm flow rate. Green arrows indicate the direction of oxygen flow.

but not within the bulk of the scale. Cracks in the oxide can be seen highlighted with the $^{18}O_2$ signal.

b. Ta Oxidation in Molecular and Atomic Oxygen

Figure 8 shows fracture cross sections of samples oxidized at 1300°C in the RHS and in the MRHS in MO only. Oxides grown on both materials are similar, with differences attributable to flow rate and flow direction. The thicknesses of the bottom oxides are similar (~30μm). Figure 9 shows temperature versus time and resistive current versus time for Ta samples oxidized at 1300°C in the MRHS in MO only and in MO+AO. The temperature versus time data shows that the MRHS can hold samples within ±20°C. The slope of the resistive current data shows that, despite the temperatures being the same for oxidation in MO and MO+AO, the current needed to maintain 1300°C decreases more when AO is present in the chamber. Figure 10 shows fracture cross sections of Ta oxidized at 1300-1500°C for 5 min in (top) MO only and (bottom) MO+AO. The oxides grown at 1300°C and 1400°C are significantly larger in MO+AO environments than in MO only. However, at 1500°C, the oxides are nearly identical between MO+AO containing an MO only.

Discussion

a. Ta and TaC Oxidation in the RHS

While the oxidation kinetics with respect to time could be fit to several rate laws, all most strongly correlated with linear oxidation. Thus, oxidation will be assumed linear for this discussion. A linear oxidation rate either implies a reaction-controlled process or gas-

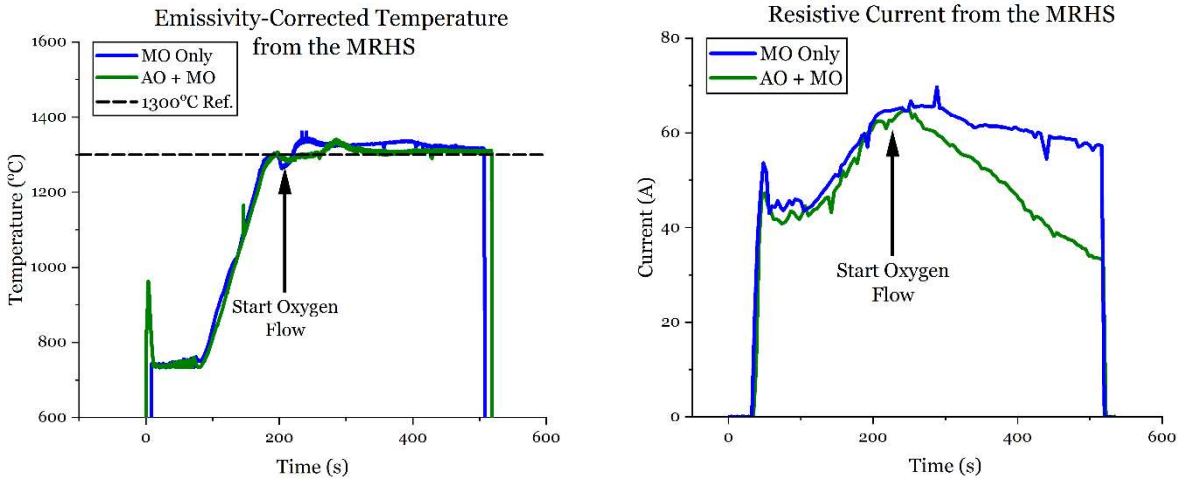

Figure 9: Temperature and resistive current data from the MRHS. Ta exposed to AO has a much steeper slope in resistive current (i.e. oxidation rate) at roughly the same oxidation temperature. Oxidation conditions are 1300°C, 5min, 100 sccm flow of 1% O_2-Ar, 65 torr Ar background

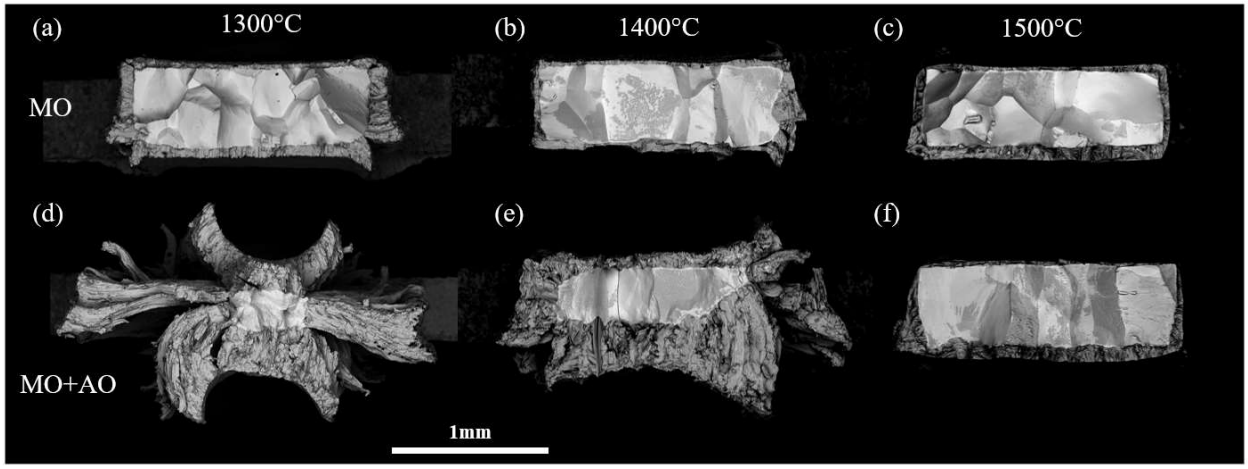

Figure 10: Backscatter SEM fracture cross section micrographs of Ta oxidized in (a-c) MO only and in (d-f) MO+AO in the MRHS. Oxidized for 5 min at (a,d) 1300°C, (b,e) 1400°C, and (c,f) 1500 C in 1% O_2 – Ar (total O content). Flow frate from MP capillary (on or off) is 100 sccm.

phase diffusion process limited by transport through large defects in the scale. The 1%O_2 environment was chosen specifically to prevent reaction-controlled oxidation, so oxygen is likely ingressing through large defects in the oxide. It can be seen that the oxidation rate of Ta is faster than the oxidation rate of TaC at 1300°C, but slower at 1400°C and 1500°C.

For Ta, the TOF-SIMS data (Figure 7) shows that oxygen travels through cracks in the oxide, which agrees with oxygen ingress via large defects. For TaC, it was expected that oxidation would be parabolic, as is characteristic of gas-phase diffusion through a porous oxide. However, the linear oxidation kinetics imply that oxygen transport occurs via large defects as well. It is hypothesized that the large voids in the scales are the primary route for oxygen ingress through the scale on TaC. TOF-SIMS has not yet been conducted on TaC to confirm this.

As temperature increases, the oxidation rate of Ta decreases. This is counterintuitive, as oxidation usually increases with increasing temperature, as is the case for TaC. This indicates that the oxide on Ta is becoming more protective at higher temperatures. The cross-section micrographs in Figure 5 support this, as the degree of cracking in the oxide on Ta decreases as temperature increases. Some mechanism either repairs the cracks after they form or prevents cracking in the first place. For TaC, the oxide becomes less porous as temperature increases, but some pores and voids persist at all temperatures. When viewed in plan view, the oxide shows small, well-rounded grains. This is not seen in the oxide on Ta. Regardless, the oxide on Ta is becoming more protective at higher temperatures. CO(g) production during carbon oxidation leads to significant amounts of pores and voids in the scale which may prevent the oxide from cracking at 1300°C like the oxide on Ta, but which prevent the oxide from becoming wholly protective as temperature increases. The data provided here is not sufficient to draw conclusions about the exact mechanism causing the increase in oxide scale protectiveness on Ta or TaC.

b. Ta Oxidation in Molecular and Atomic Oxygen

Figures 8-10 show the success of the new MRHS system as a tool for high temperature oxidation studies. Additionally, they highlight that AO can successfully be produced and used in oxidation studies via the MRHS. The micrographs in Figure 8 show that the oxides which form on Ta are very similar whether oxidation by MO is carried out in the RHS or MRHS. The oxides on the bottom of the samples (facing the MP jet) have similar thicknesses (~30μm). The thickness of the oxide on the remaining sides of the sample exposed in the RHS is greater than that of the MRHS. However, the flow rate in the RHS is 10 times higher and the system is at atmospheric pressures, while the MRHS had reduced pressure (65 torr) for MP operation. The capabilities of the RHS have previously

been verified compared to traditional furnaces[31]. The comparable thickness of the oxide on the bottom of the sample implies that oxidation in the MRHS is also comparable to other traditional furnaces. The oxides on the bottom of the samples will be used for further characterization of these samples.

The slopes in resistive current versus time plot (Figure 9) are indicative of oxidation rate. The amount of Joule heating is indirectly proportional to the cross-sectional area of the substrate. Thus, as the sample oxidizes, the cross-sectional area decreases, and the amount of current required to maintain a constant temperature decreases. It can clearly be seen that the Ta sample exposed to AO+MO has a much steeper slope than the sample exposed to MO only. This implies a greater oxidation rate when AO is present, which is reflected by the micrographs in Figure 10. The oxides formed on Ta when exposed to 1300°C and 1400°C, which were previously shown to be non-protective due to cracks in the oxide, show significantly thicker oxides when oxidized in AO. AO likely travels through the cracks without recombining to MO and reacts with the base Ta. This can be seen especially in Figure 10e, where one corner of the base Ta has been completely consumed. In contrast, the oxide grown at 1500°C shows nearly identical oxides in both MO only and AO+MO exposures. This is because at 1500°C, the oxide becomes more protective and prevents rapid oxygen ingress through the scale. Cracks are either smaller or entirely absent, so AO cannot reach the surface of the metal without recombining to MO or adsorbing to the oxide. As such, AO can be used as a "leak detector", showing when the oxide formed on Ta is protective or non-protective by finding cracks in the oxide.

Conclusions

The oxidation of Ta and TaC were explored at 1300-1500°C to elucidate the role of carbon on oxygen transport through the scale. Ta was found to oxidize faster than TaC at 1300°C, despite the porous oxide formed on TaC. This is due to cracks in the oxide on Ta which allow rapid oxygen ingress to the metal surface. The evolution of CO(g) during TaC oxidation creates a highly porous oxide with large voids interspersed throughout. These voids may be the primary oxygen ingress pathway, as oxidation proceeds with linear rather than parabolic kinetics. These voids may also help prevent cracking, but ultimately undermine the protectiveness of the scale as temperature increases to 1500°C.

A new microplasma resistive heating system was constructed and used to conduct oxidation experiments on Ta in molecular oxygen (MO) and atomic oxygen (AO). Oxidation was found to be more rapid when AO was present and the oxide on Ta was non-protective, indicating that AO is able to diffuse through bulk defects in the oxide to arrive at and react with the metal. When the oxide is more protective, AO cannot arrive at the surface without reacting with the oxide or recombining to MO. The oxidation rate of Ta in AO with a more protective oxide (1500°C) appears the same as oxidation in MO.

Future Work

Additional "double oxidation" studies and TOF-SIMS analysis on Ta and TaC are planned to better characterize the oxygen ingress pathway. Experiments varying the oxygen partial pressure are planned to see if the transport changes with P_{O_2}. Oxidation experiments at 1600°C are also planned to see if the protectiveness of the oxide continues to improve at higher temperatures.

This work is part of a project exploring the oxidation of transition metals and metal carbides (M = Ti, Zr, Hf, Ta) at high temperatures and in MO and AO. The Ta/TaC and Zr/ZrC systems have been well characterized, but more work on Ti/TiC and Hf/HfC is needed. Group IV carbides form "oxycarbide" intermediate layers which change the mechanism for oxygen ingress. Characterization of these systems via the methods described above is ongoing. "Double oxidation" and TOF-SIMS analysis are planned to better understand the oxygen ingress pathways for these materials.

The recent completion of the MRHS has also opened the door to conduct MO versus AO experiments on other materials as well. This has only been conducted for Ta thus far but will also continue for the other metals and carbides discussed.

Acknowledgements

The author would like to thank: Mr. Steve DiPietro and Exothermics, Inc. for providing the Ta; Dr. H. Heinrich for assisting with the

FIB, HRTEM, and SAED; Dr. M. Gordon for helpful discussion and advice in constructing the microplasma system; Ms. S. Donaldson for help investigating the dissociation fraction of the microplasma; Mr. C. Recupero, Ms. A. Uy, and Mr. M. Richwine for assistance in lab work; and Dr. E. Opila for her guidance and patience during this process.

Use of the Quanta 650 FEG-SEM and the Empyrean Diffractometer was possible through the University of Virginia Nanoscale Materials Characterization Facility (NMCF).

This project was funded by the Air Force Office of Scientific Research (AFOSR). Funding for the construction of the M-RHS was provided by the AFOSR Defense University Research Instrumentation Program (DURIP). Additional resources were provided by the Virginia Space Grant Consortium (VSGC) Graduate Student Fellowship Program.

References

1. Wuchina, E., Opila, E. J., Opeka, M. M., Fahrenholtz, W. & Talmy, I. G. (2007).
2. Opeka, M. M., Talmy, I. G. & Zaykoski, J. A. *J Mater Sci* **39**, 5887–5904 (2004).
3. Choi, G. M. & Tuller, H. 1. *J. Am. Ceram. Soc.* **73**, 1700-1704, (1990).
4. Kofstad, P. & Ruzicka, D. J. *J. Electrochem. Soc.* (1963).
5. Desmaison-Brut, M., Alexandre, N. & Desmaison, J. *J. Euro. Ceram. Soc.* vol. 17 1325–1334, (1997).
6. Scott, J. A., He, X. & Lipke, D. W. *J. Amer. Ceram. Soc.* (2022) doi:10.1111/jace.18941.
7. Voitovich, V. B. *High Temperature Materials and Processes* **16**, 243–253 (1997).
8. Courtright, E. L., Prater, J. T., Holcomb, G. R., St. Pierre, G. R. & Rapp, R. A. *Oxidation of Metals* **36**, 423–437 (1991).
9. Stringer, J. *Acta. Met.* **8**, 758–766 (1960).
10. Toffolon-Masclet, C., Desgranges, C., Corvalan-Moya, C. & Brachet, J. C. *Solid State Phenomena* 652–657 (2011).
11. Sharma, G., Ushakov, S. V. & Navrotsky, A. *J. Amer. Ceram. Soc.* **101**, 31–35 (2018).
12. Kofstad, P. *Journal of The Less-Common Metals* **12**, 449–464 (1967).
13. Kofstad, P. *Journal of The Less-Common Metals* **7**, 241–266 (1964).
14. Bargeron, C. B., Benson, R. C., Jette, A. N. & Phillips, T. E. *J. Amer. Ceram. Soc.* **76**, 1040–1046 (1993).
15. Gasparrini, C., Podor, R., Horlait, D., Chater, R. & Lee, W. E. *Oxidation of Metals* **88**, 509–519 (2017).
16. Gasparrini, C., Chater, R. J., Horlait, D., Vandeperre, L. & Lee, W. E. *J. Amer. Ceram. Soc.* **101**, 2638–2652 (2018).
17. Lavrenko, V. A., Glebov, L. A., Pomitkin, A. P., Chuprina, V. G. & Protsenko, T. G. *Oxidation of Metals* **9** (1975).
18. Tolpygo, V. K. & Clarke, D. R. *Acta mater.* **46**, 5153–5166 (1998).
19. Clarke, D. R. *Current Opinion in Solid State and Materials Science* **6** (2002).
20. Rhines, F. N. & Wolf, J. S. *Metallurgical Trans*. **1**, (1970)
21. Lashtabeg, A., Smart, M., Riley, D., Gillen, A. & Drennan, J. *J Mater Sci* **48**, 258–264 (2013).
22. Berkowitz-Mattuck, J. B. *J Electrochem Soc* **114**, 1030–1033 (1967).
23. Primc, G., Zaplotnik, R., Vesel, A. & Mozetic, M. *AIP Adv* **1**, (2011).
24. Balat, M., Flamant, G., Male, G. & Pichelin, G. *Journal of Materials Science* **27** (1992).
25. Monteverde, F. & Savino, R. *J Eur Ceram Soc* **27**, 4797–4805 (2007).
26. Marschall, J. *et al.* Oxidation of ZrB2–SiC *J Thermophys. Heat Trans* **23**, 267–278 (2009).
27. Li, N., Hu, P., Zhang, X., Liu, Y. & Han, W. *Corros Sci* **73**, 44–53 (2013).
28. Rosner, D. E. & Allendorf, H. D. *J Electrochem Soc* **114**, 305 (1967).
29. Rosner, D. E. & Allendorf, H. D. *Carbon N Y* **3**, 153–156 (1965).
30. Karlsdottir, S. N. & Halloran, J. W. *J. Amer. Ceram. Soc.* **90**, 3233–3238 (2007).
31. Shugart, K., Patterson, B., Lichtman, D., Liu, S. & Opila, E. *J. Amer. Ceram. Soc.* **97**, 2279–2285 (2014).
32. Mariotti, D. & Sankaran, R. M. *J Phys D Appl Phys* **43**, (2010).
33. Buczala, D. M., Brunsvold, A. L. & Minton, T. K. *J Spacecr Rockets* **43**, 421–425 (2006).
34. Koh, T. L., O'Hara, E. C. & Gordon, M. J. *Nanotechnology* **23**, (2012).
35. Koh, T. L. & Gordon, M. J. *J Phys D Appl Phys* **46**, (2013).
36. Kofstad, P. *Journal of the Less Common Metals* **5**, 158–170 (1963).
37. Schneider, C., Rasband, W. & Eliceiri, K. *Nat Methods* **9**, 671–675 (2012).